

Chiral Spin States in a Spin-charge Coupled System on the Shastry-Sutherland Lattice

Munir Shahzad and Pinaki Sengupta

School of Physical and Mathematical Sciences, Nanyang Technological University, 21 Nanyang Link, Singapore 637371

(Dated: May 17, 2022)

We investigate the necessary conditions for the emergence of complex, non-coplanar magnetic configurations in a Kondo lattice model with classical local moments on the geometrically frustrated Shastry-Sutherland lattice, and their evolution in an external magnetic field. We demonstrate that topologically non-trivial spin textures – including a new *canted flux* state – with non-zero scalar chirality arise dynamically from realistic short range interactions. Our results establish that a finite Dzyaloshinskii-Moriya (DM) interaction is necessary for the emergence of these novel magnetic states when the system is at half-filling for which the ground state is insulating. We identify the minimal set of DM vectors that are necessary for the stabilization of chiral magnetic phases. Furthermore, the non-coplanarity of such structures can be tuned continually by applying an external magnetic field. Once again, the nature of the DM interactions dictate the emergence of magnetization plateaus that are ubiquitous in the canonical Shastry-Sutherland model. Our results are crucial in understanding the magnetic and electronic properties of the rare earth tetraboride family of frustrated metallic magnets.

I. INTRODUCTION

The study of strongly interacting quantum many body systems with independent spin and charge degrees of freedom on frustrated lattices have attracted heightened interest in the recent past. The interplay between geometric frustration and strong interaction between itinerant electrons and localized moments in these systems results in novel quantum phases and phenomena that are not observed in their non-frustrated counterparts^{1–8}. Frustrated interactions between the local moments, together with crystal electric fields and coupling to the itinerant electrons, often stabilize non-coplanar ordering of these moments^{1,9–12}. When an electron moves through such background spin textures, it picks up a Berry phase which underlies several novel transport phenomena such as the topological (or geometric) Hall effect and unconventional magnetoresistive properties^{13–16}. The interest in these systems is driven both by the desire to understand the underlying mechanism driving the novel phenomena as well as to control their emergence by external tuning fields in order to harness their unique functionalities for practical applications.

In this paper, we study the Kondo Lattice Model (KLM) on the geometrically frustrated Shastry-Sutherland lattice (SSL) with classical spins where the standard (antiferromagnetic) Heisenberg interaction between the local moments is supplemented by an additional Dzyaloshinskii-Moriya (DM) interaction. The SSL is a paradigmatic geometry to study the effects of competing interactions in the presence of frustration¹⁷. The Shastry-Sutherland Kondo lattice model (SS-KLM) has previously been studied with $S = 1/2$ local moments^{18–21} where quantum fluctuations of the local moments play a crucial role in determining the character of the ground state. In the present study, we revisit this model, but with the local moments treated as classical spins. This is not simply of academic interest. There exist a complete family of rare-earth tetraborides (RB_4 , $\text{R}=\text{Tm}$, Er , Ho , Dy) – quasi-two-dimensional metallic magnets where the magnetic moment-carrying rare

earth ions are arranged in a SSL in the layers. Due to strong spin-orbit coupling, the rare-earth ions in these compounds carry large magnetic moments and consequently, can be treated as classical spins. They act as effective local fields that interact strongly with the electron spin.^{22–29} In this study our goal is to construct a minimal model where topologically non-trivial chiral magnetic phases can be realized from physically relevant interactions and investigate their evolution in an external magnetic field. In particular, we explore the role of different components of the DM interaction in stabilizing different aspects of the local moment configurations. What are the minimal DM vectors required to stabilize a *tunable* non-coplanar spin configuration, as well as magnetization plateaus? How does an applied field affect the non-coplanarity of the spin configuration? Does the *nature* of chiral spin state change in the presence of an external field? These are some of the questions we address in this work. Our results reveal that multiple non-coplanar spin arrangements (characterized by different values of the scalar spin chirality) with long range magnetic order are stabilized over an extended range of parameters. Not surprisingly, we find that DM interactions play a crucial role in stabilizing chiral spin configurations. Furthermore, we are able to tune the non-coplanarity (equivalently, the topological character) of the spin textures – changing and suppressing the net chirality – by applying an external magnetic field. This is in contrast to most previous studies where the non-coplanar textures of the local moments is imposed by extraneous factors (e.g., crystal electric field in pyrochlores) and as such, cannot be changed easily.

II. MODEL

The Hamiltonian describing the SS-KLM with additional DM interactions is given by,

$$\mathcal{H} = \mathcal{H}_e + \mathcal{H}_{ex} + \mathcal{H}_{DM} + \mathcal{H}_H \quad (1)$$

where \mathcal{H}_e represents the electronic Hamiltonian,

$$\mathcal{H}_e = - \sum_{\langle i,j \rangle, \sigma} t_{ij} (c_{i\sigma}^\dagger c_{j\sigma} + h.c.) - J_K \sum_i \mathbf{S}_i \cdot \mathbf{s}_i$$

The first term is the kinetic energy of the itinerant electrons – $\langle i, j \rangle$ represents the Shastry-Sutherland bonds (viz., first neighbors along the principal axes and the alternate diagonals) and t_{ij} are the transfer integrals for these bonds. The second term is the on-site Kondo-like interaction between the spin of the itinerant electrons \mathbf{s}_i and localized moments \mathbf{S}_i . The conduction electron spin is defined as $\mathbf{s}_i = c_{i,\alpha}^\dagger \boldsymbol{\sigma}_{\alpha\beta} c_{i,\beta}$, where $\boldsymbol{\sigma}_{\alpha\beta}$ is the vector element of usual Pauli matrices. As mentioned in the introduction we treat the localized spins as classical vectors with unit length ($|\mathbf{S}_i| = 1$). In this limit, the sign of J_K (ferromagnetic or antiferromagnetic) is irrelevant since eigenstates that correspond to different signs are related by a global gauge transformation. The states of the localized spins are specified by the angular components as $\mathbf{S}_i = (\sin \theta_i \cos \phi_i, \sin \theta_i \sin \phi_i, \cos \theta_i)$. Among the other terms in Eq. (1) \mathcal{H}_{ex} represents the classical Heisenberg interaction between the localized spins, $\mathcal{H}_{ex} = \sum_{\langle i,j \rangle} J_{ij} \mathbf{S}_i \cdot \mathbf{S}_j$. \mathcal{H}_{DM} describes the Dzyaloshinskii-Moriya (DM) interaction, $\mathcal{H}_{DM} = \sum_{\langle i,j \rangle} \mathbf{D}_{ij} \cdot (\mathbf{S}_i \times \mathbf{S}_j)$, where \mathbf{D}_{ij} is the DM vector which is determined by the crystal symmetry of the lattice. The precise values (directions and magnitude) DM vectors will depend on the details of the crystal symmetry for each compound. In this study we choose a generic set of DM vectors and identify the minimal interactions that are necessary for stabilizing non-coplanar spin textures. The explicit form of the DM vectors on the different bonds is given in the caption of Fig. 1. The last term in the Hamiltonian (1) is the Zeeman term for the localized spins due to an external (longitudinal) magnetic field, $\mathcal{H}_H = -h^z \sum_i S_i^z$. A Zeeman term for the itinerant electrons is not included explicitly, since the instantaneous spin orientation of the electrons are determined completely by the local moments in the large J_K limit that we consider in this study. Hereafter the parameters with primes represent the interactions on diagonal bonds while the unprimed are for axial bonds.

III. METHOD AND OBSERVABLES

To investigate the above model, we use an unbiased Monte Carlo (MC) method that has been used previously in the study of similar models^{5,30–32}. A brief review of this method is presented here closely following the references^{33,34}. The dynamics of large localized moments of the rare earth ions is slow compared to itinerant electrons and, accordingly, we can decouple their dynamics from that of the itinerant electrons. While studying the latter, we treat the local moments as static, classical fields at each site. The electronic part of the Hamiltonian is bilinear in fermionic operators. Using the single electron basis, \mathcal{H}^e can be represented as $2N \times 2N$ matrix for a fixed configuration of classical localized spins, where N is the number of sites.

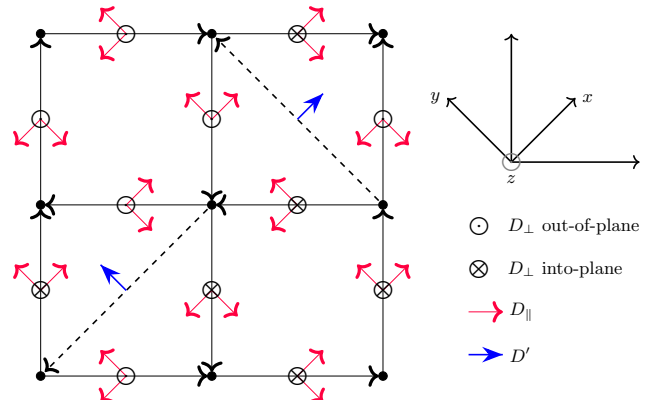


FIG. 1. (Color online) DM interaction defined on the unit cell of SSL where directions of the arrow from site i to j indicates the direction of cross product $\mathbf{S}_i \times \mathbf{S}_j$. The red arrows represent the parallel components of \mathbf{D} while \ominus and \otimes represent out-of-plane and into components of \mathbf{D} . Blue arrows indicate the components of \mathbf{D}' on the diagonal bonds. The directions of x , y and z axis are also mentioned.

In order to explore the thermodynamic properties we write the partition function for the whole system by taking two traces,

$$Z = \text{Tr}_S \text{Tr}_I \exp[-\beta(\mathcal{H}^e(\{x_r\}) - \mu \hat{N}_e)] \cdot \exp[-\beta(\mathcal{H}_{ex} + \mathcal{H}_{DM} + \mathcal{H}_H)] \quad (2)$$

where Tr_S and Tr_I represent the traces over the classical localized spins denoted by $\{x_r\}$ and the charge degrees of freedom respectively. The trace over itinerant electron degrees can easily be calculated by numerical diagonalization Hamiltonian matrix \mathcal{H}^e for a fixed configuration of localized spins $\{x_r\}$,

$$\text{Tr}_I \exp[-\beta(\mathcal{H}^e(\{x_r\}) - \mu \hat{N}_e)] = \prod_\nu (1 + \exp[-\beta(\varepsilon_\nu(\{x_r\}) - \mu)]) \quad (3)$$

where μ is the chemical potential, $\beta = 1/k_B T$ is the inverse temperature and $\hat{N}_e = \frac{1}{2N} \sum_{i\sigma} c_{i\sigma}^\dagger c_{i\sigma}$ is the number density of conduction electrons. The partition function for the whole system then takes the form,

$$Z = \text{Tr}_S \exp[-S_{eff}(\{x_r\}) - \beta(\mathcal{H}_{ex} + \mathcal{H}_{DM} + \mathcal{H}_H)] \quad (4)$$

The corresponding effective action is $S_{eff}(\{x_r\}) = \sum_\nu F(y)$ where $F(y) = -\log[1 + \exp\{-\beta(y - \mu)\}]$. The grand canonical trace over localized spin degrees of freedom is evaluated by sampling the spin configuration space using a classical Monte Carlo (MC) method. The probability distribution for a particular configuration of localized spins $\{x_r\}$ can be written as,

$$P(\{x_r\}) \propto \exp[-S_{eff}(\{x_r\}) - \beta(\mathcal{H}_{ex} + \mathcal{H}_{DM} + \mathcal{H}_H)] \quad (5)$$

The thermodynamic quantities that depend on localized spins are calculated by the thermal averages of spin

configurations while the quantities that are associated with itinerant electrons are calculated from the eigenvalues and eigenfunctions of $\mathcal{H}^e(\{x_r\})$. We start the simulations with a random configuration of localized spins $\{x_r\}$ and calculate Boltzmann action $S_{\text{eff}}(\{x_r\})$ for this configuration. The spin configuration is updated via Metropolis algorithm based on the change in the effective actions of the configurations resulting from random updates, $\Delta S_{\text{eff}} = S_{\text{eff}}(\{x'_r\}) - S_{\text{eff}}(\{x_r\})$. To identify magnetic orderings we calculate the magnetization per unit site as well as spin structure factor which is the Fourier transform of the spin-spin correlation function,

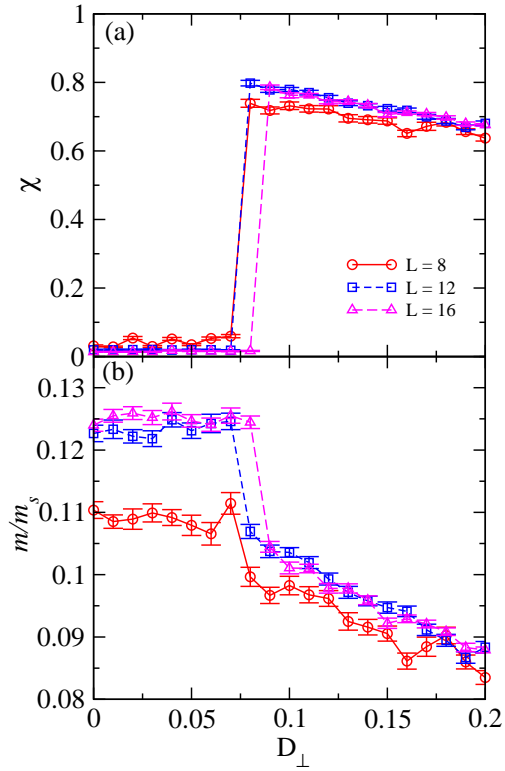


FIG. 2. (Color online) (a) Chirality per unit cell and (b) magnetization per unit site as a function of D_{\perp} for 8×8 , 12×12 and 16×16 lattice sizes. The results are obtained at $T = 0.02$ while keeping $t = 1.0$, $t' = 1.2$, $J = 0.1$, $J' = 0.12$, $J_K = 3.0$, $D_{\parallel} = 0.0$, $D' = 0.0$ and $h^z = 0.0$.

$$S(\mathbf{q}) = \frac{1}{N} \sum_{i,j} \langle \mathbf{S}_i \cdot \mathbf{S}_j \rangle \exp[i\mathbf{q} \cdot \mathbf{r}_{ij}] \quad (6)$$

where \mathbf{r}_{ij} is the position vector from i^{th} to j^{th} site and $\langle \rangle$ represent the thermal averages over the grand canonical ensemble. To elucidate the difference between topological trivial and non-trivial states we evaluate the local scalar chirality. On a triangle the chirality is defined as,

$$\chi_{\triangle} = \mathbf{S}_i \cdot (\mathbf{S}_j \times \mathbf{S}_k) \quad (7)$$

We use the total chirality $\chi = \frac{1}{N_u} \sum_{\triangle} \chi_{\triangle}$ (where sum is over all the triangles formed on the plaquettes with diagonal bonds and N_u is the number of unit cells of

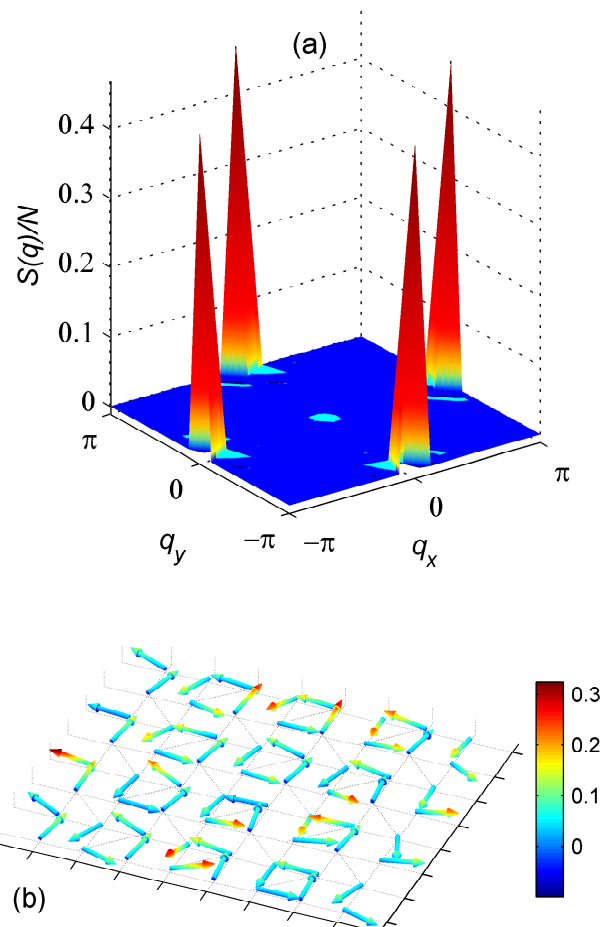


FIG. 3. (Color online) (a) Plot of spin structure factor along q_x and q_y indicating the two sharp peaks appearing at $\mathbf{q} = (0, \pi)$ and $(\pi, 0)$ and a small peak at $\mathbf{q} = (0, 0)$ for 16×16 lattice. (b) The snapshot of real space localized spin configuration for 8×8 lattice showing the canted flux state. The MC calculations are done keeping $T = 0.02$, $t = 1.0$, $t' = 1.2$, $J = 0.1$, $J' = 0.12$, $J_K = 3.0$, $D_{\parallel} = 0.0$, $D' = 0.0$ and $h^z = 0.0$.

SSL) as the chiral order parameter. This quantity is zero for collinear or coplanar magnetic states such as ferromagnetic (FM), anti ferromagnetic (AFM) and pure flux states whereas it is non-zero for *non-coplanar* configurations, e.g., all-out and 3-in 1-out states observed in pyrochlores. Finally, as an additional characterization of the chiral nature of the spin configurations, we measure the circulation of the in-plane components around each square palquette as $f_m = \sum_{\square} \mathbf{S}_i \cdot \mathbf{r}_{ij}$, where \mathbf{S}_i is the spin at site i and \mathbf{r}_{ij} 's are the vectors connecting sites i and j around the square plaquette in a counter-clockwise direction. A non-zero circulation identifies a flux configuration of the local moments.

IV. RESULTS

Simulations of the hamiltonian (1) were performed in lattices of dimension $L \times L$ with $L = 8 - 16$, over a

wide range of parameters. For smaller lattices, we used exact diagonalization- Monte Carlo (ED-MC) method where the full Hamiltonian is diagonalized to calculate the effective action for each MC step. For the larger lattices, we used travelling cluster approximation (TCA) method^{35–38} – a 6×6 cluster of SSL is used to calculate the effective action for one MC sweep. Once the system is equilibrated then we calculated the thermal averages by diagonalizing the full Hamiltonian matrix. To avoid getting trapped in local minima and to speed up the equilibration, we used simulated annealing. For this, we start the simulations at a relatively high temperature $T = 0.1$ with random localized spin configuration and run the system for equilibration and then use final configuration at this temperature to do the equilibration at $T = 0.08$. We repeat this process with a step of temperature $\Delta T = 0.02$ finally calculating the thermal averages of the observables at temperature $T = 0.02$. For the lattice sizes studied, the thermal gap to the lowest excitation is greater than the finite size gap at $T = 0.02$. In other words, $T = 0.02$ is sufficiently small such that ground state estimates of the measured observables can be reliably obtained. Measurements are done for 40,000 MC steps after 2000 – 60,000 steps for thermalization.

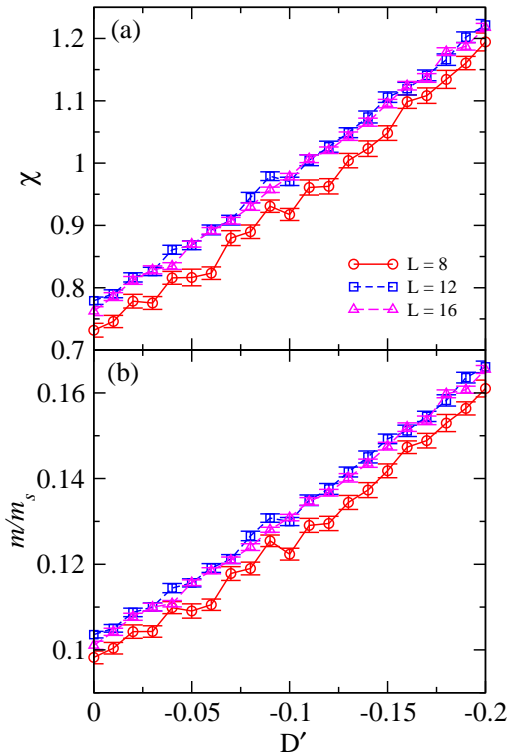


FIG. 4. (Color online) (a) Chirality per unit cell and (b) magnetization per unit site as a function of D' for 8×8 , 12×12 and 16×16 lattice sizes. The calculations are obtained at $T = 0.02$, $t = 1.0$, $t' = 1.2$, $J = 0.1$, $J' = 0.12$, $J_K = 3.0$, $D_{\parallel} = 0.0$, $D_{\perp} = 0.10$ and $h^z = 0.0$.

With its multi-dimensional parameter space, the Hamiltonian (1) is expected to support a rich array of ground state phases over different ranges of the parameters. In the present work, we restrict our attention

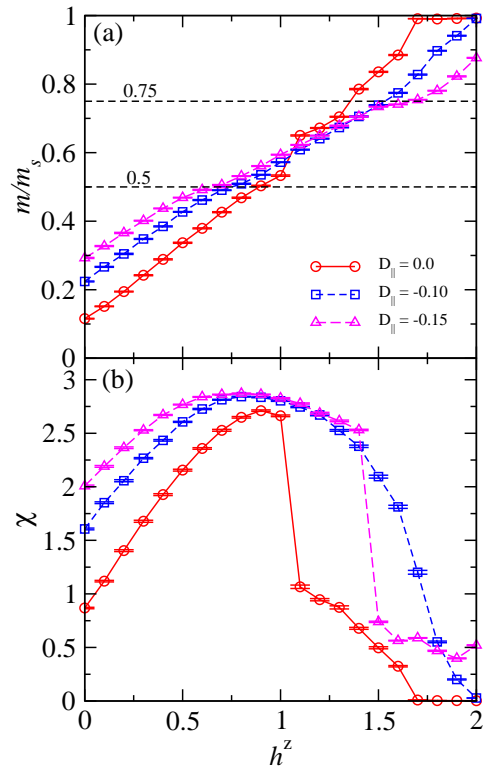


FIG. 5. (Color online) (a) Magnetization per unit site and (b) chirality per unit cell as a function of external magnetic field for different values of D_{\parallel} . The results are obtained for 12×12 at $T = 0.02$, $t = 1.0$, $t' = 1.2$, $J = 0.1$, $J' = 0.12$, $J_K = 3.0$, $D_{\perp} = 0.10$ and $D' = -0.05$.

on the magnetic behavior at an electronic filling factor $\langle N_e \rangle = 1/2$, for which the system is in an insulating state. The choice for the rest of the Hamiltonian parameters are guided by experimental observation in real materials. The electronic hopping matrix elements along the axial bonds are chosen as $t = 1.0$ – this sets the energy scale for the problem. The diagonal hopping is set to $t' = 1.2$ and the values of the exchange interactions along the axial and diagonal bonds are set at $J = 0.1$ and $J' = 0.12$. This choice is motivated by the experimental observation of approximately equal bond lengths in the rare earth tetraboride family of compounds. In most materials of relevance to the present model, there exist strong DM interactions. While the exact nature of DM interaction depends on the crystal symmetries, we have chosen a generic form of DM interaction for our study. Indeed, investigating the role of DM interaction in stabilizing non-coplanar spin configurations is a central goal of the present study. Finally, following the experimental observation in other frustrated metallic magnets such as the pyrochlores, the strength of the Kondo coupling is chosen to be the strongest energy scale in the problem, $J_K = 3.0$.

A. Effect of DM interaction

In the first part of the study, a systematic variation of the different components of the DM vector is performed to identify the minimal set of vectors necessary for non-coplanar configurations of the local moments. We study the effects of the DM vectors normal to the plane of the lattice, D_{\perp} , and two in-plane components, D_{\parallel} and D' (fig.1). It is found that while D_{\perp} is essential for the emergence of non-coplanarity, D_{\parallel} drives the appearance of field induced magnetization plateaus.

1. Role of D_{\perp}

We start our discussion by analyzing the nature of the magnetic ground state at zero field. The evolution

of chirality as D_{\perp} is varied is shown in Fig. 2(a). At $D_{\perp} = 0$, the ground state has predominantly longitudinal AFM order with a vanishingly small chirality. There is a small, but non-zero uniform magnetization – a consequence of large Kondo-like coupling between the charge and spin degrees of freedom. With increasing the value of D_{\perp} , the ground state remains in the same phase with vanishing chirality up to a critical value ≈ 0.8 beyond which there is a discontinuous transition to a chiral state characterized by a finite value of χ . This is accompanied by a sharp drop in the uniform magnetization [see Fig. 2(a)]. The sharp increase in chirality indicates a non-coplanar component to the spin configuration and establishes topologically non-trivial nature of the spin configuration.

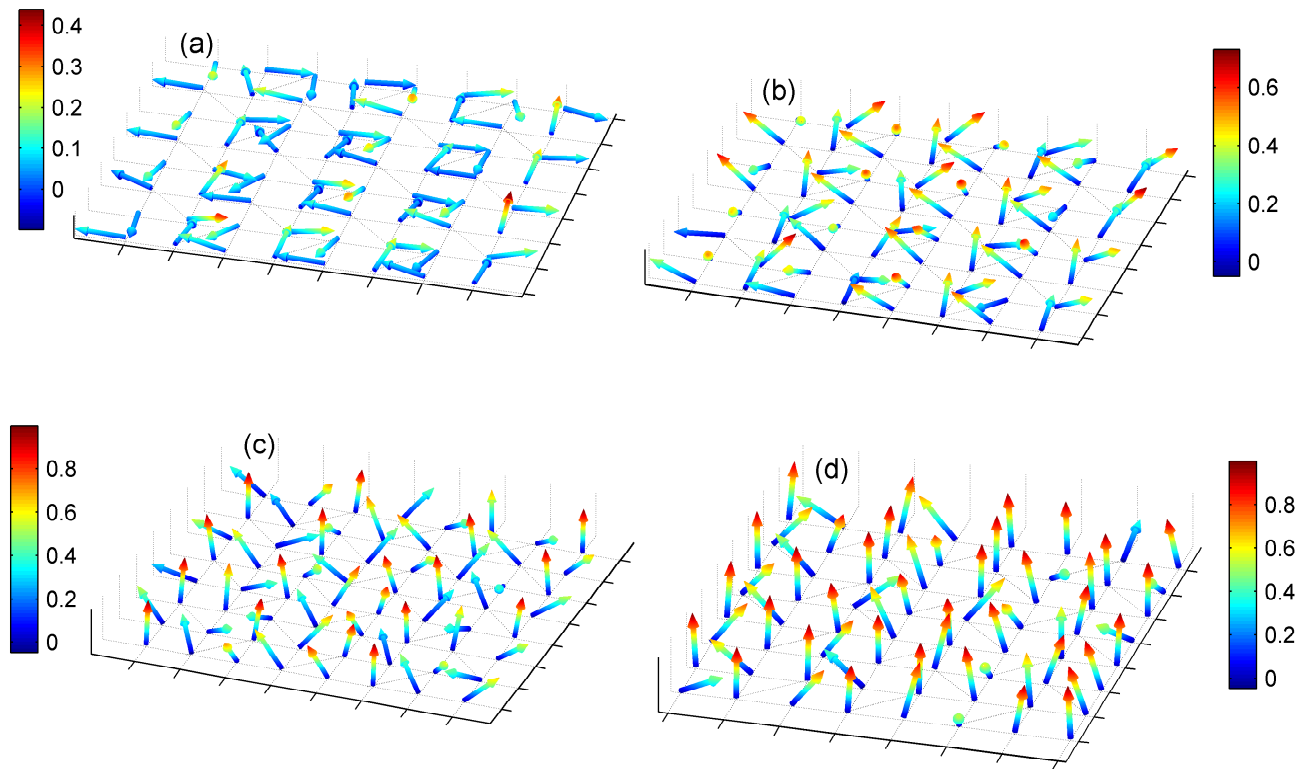


FIG. 6. (Color online) The real space configurations of local spins for 8×8 lattice shown at different values of magnetic field (a) $h_z = 0.0$ (b) $h_z = 0.8$, just prior to a phase transition (c) $h_z = 1.2$, after the phase transition point and (d) $h_z = 1.6$, when local spins are almost becoming polarized with magnetic field. The colorbar besides each plot indicates the out of plane component of the spin vector. The MC simulations are performed at $T = 0.02$, $t = 1.0$, $t' = 1.2$, $J = 0.1$, $J' = 0.12$, $J_K = 3.0$, $D_{\parallel} = 0.0$, $D_{\perp} = 0.1$ and $D' = -0.05$.

Additional insight into the magnetic ground state can be obtained from the momentum dependence of the static spin structure factor which is illustrated in Fig. 3(a). It exhibits sharp peaks at $(\pi, 0)$ and $(0, \pi)$. There is an additional, sub-dominant peak at $(0, 0)$ indicating a net magnetic moment even at zero external field [see Fig. 2(b)], despite the AFM nature of the Heisenberg interaction between the localized moments. This is due to both the DM interaction which favors an out-

of-plane orientation of the spins, as well as the interaction between the local moments and the spin of the itinerant electrons. Nominally such features in the structure factor points towards a canted antiferromagnetic state. However, that is not the case here. The true nature of the non-coplanar ground state is illustrated by a snapshot of the real space (periodic) equilibrium spin configuration obtained from the simulations and shown schematically in Fig. 3(b). The in-plane components of

the local moments are arranged in a near-ideal flux pattern along with a finite out-of-plane component – that is, the magnetic ground state is a canted flux state. Such complex spin textures are essential ingredients for the observation of topological Hall effect, chiral spin liquid and other topologically interesting phases. In contrast to pyrochlores where the non-coplanar terahedral ordering of the local moments is fixed by the crystal field effects, the canted flux state in our study arise dynamically from the interplay between competing Heisenberg, DM and Kondo-like interactions in the presence of geometric frustration. This enables us to control these complex magnetic orderings continually via an external magnetic field.

2. Role of D'

After finding the minimum value of D_{\perp} that causes the topological non-trivial phase transition we discuss the effect of D' on the non-coplanar ground state. The results for chirality and magnetization per unit site as a function of D' are shown in Fig. 4 (a) and (b). The increase in D' results in an enlarged out-of-plane component of the localized spins making the ground state more canted. Hence with the increase of D' the non-coplanarity of the magnetic ordered state increases [see Fig 4(a)]. The same effect is observed in the behavior of the magnetization per unit site – magnetization increases monotonically with D' as the enlarged out-of-plane component of spins contributes to increase in zero field magnetization [see shown in Fig. 4(b)]. The static spin structure factor $S(\mathbf{q})$ at $D' = -0.10$ (not shown here) confirms that the magnitude of the peak at $q = (0, 0)$ is higher than that without D' . Similarly, a plot of the real space snapshot of the ground state (not shown here) shows that canting of spins increase with the introduction of D' . It is worth mentioning that D' can not induce the chiral phase transition on its own – one always needs a non-zero value of D_{\perp} for that.

3. Role of $D_{\parallel}(h_z = 0)$

Like D' , the other in-plane component of the DM vector (D_{\parallel}) cannot induce non-coplanarity of the spin configurations by itself. Instead, it simply reinforces such configurations driven by D_{\perp} (increased χ) as well as increases the uniform magnetization by enhancing the canting of the local moments away from the z -axis. However, D_{\parallel} plays a key role in driving magnetization plateaus in an external field, as detailed in the next section.

B. Effects of an external magnetic field

One of the most intriguing features of the canonical (purely magnetic) Shastry-Sutherland model is the appearance of magnetization plateaus in an applied magnetic field. It is expected that DM interactions strongly

modify the plateau structure. Our results show that the appearance and nature of the plateaus in the presence of simultaneous DM and Kondo-like interactions depend on the magnitude of D_{\perp} and D_{\parallel} . For $D_{\perp} > 0.1$ necessary to stabilize non-coplanar spin textures that we are interested in, the plateaus are completely suppressed in the absence of D_{\parallel} . For small values ($|D_{\parallel}| \lesssim 0.1$), there are no signatures of any plateau-like features in the field dependence of the uniform magnetization – m/m_s increases monotonically with increasing field strength and reaches saturation around $h_z \sim 1.7$. For $D_{\parallel} = -0.10$ signs of non-monotonicity begins to appear at $m/m_s = 0.5$ and 0.75. Further increasing the D_{\parallel} component of DM interaction two magnetization plateaus are observed at $m/m_s = 0.5$ and ~ 0.75 . The evolution of the uniform magnetization in a longitudinal magnetic field is shown in Fig. 5(a) for 3 different values of D_{\parallel} . The strongest plateau appears at $m/m_s \sim 0.75$, in contrast to all other reported magnetization plateaus (theoretical or experimental) in the spin-only Shastry-Sutherland model and associated quantum magnets. The large value of magnetization plateau is a consequence of the additional canting out of the plane driven by the coupling of the local moments with the itinerant electrons as well as the strong DM interaction. With the increase of D_{\parallel} the canting of the localized spins increases even at zero field as can be seen in Fig. 5(b) where we have plotted the chirality as a function of external field for different values of D_{\parallel} .

Finally, we discuss the topological nature of the magnetic ground state as it is tuned by an external field for a representative set of DM vectors where the zero-field ground is in a canted flux state. Fig. 5(b) shows the evolution of the net static spin chirality with increasing magnetic field. The ground state spin texture remains non-coplanar in nature over a large range of applied field strength. The chirality increases monotonically up to a critical field of $h_{c1} \approx 1.0$, above which there is a discontinuous transition to a different chiral spin state with small (but still non-zero) chirality. Eventually, when the field strength is increased beyond a second critical field $h_{c2} \approx 1.5$, the ground state loses its non-coplanarity and the chirality is completely suppressed. Once again, snapshots of local spin configurations and circulation elucidate the true nature of the magnetic ground state[see Fig. 6]. For $h^z = 0$ the circulation is equal in magnitude and opposite in sign for the plaquettes with diagonal bonds whereas it is vanishingly small in the other plaquettes. In other words, the in-plane components of the local moments are arranged in a flux pattern on alternating plaquettes. Snapshots at $h = 0.8 (< h_{c1})$ reveal that the ground state remains a canted flux state for $h \leq h_{c1}$. The discontinuous transition at h_{c1} is driven by the partial breaking of the flux configuration of the in-plane components—in other words, the transition is topological in character. The moments connected by the diagonal bonds inside the plaquettes with positive circulation still retain a large in-plane component and $(\pi, 0)$ ordering, whereas the other spins are largely polarized. The partial breaking of the flux pattern causes a drop in the circulation across the transition [Fig. 7] whereas the

polarization of half the spins results in a drop in the staggered magnetization. The transition at h_{c2} is marked by the complete breaking of the flux pattern and polarization of the remaining spins.

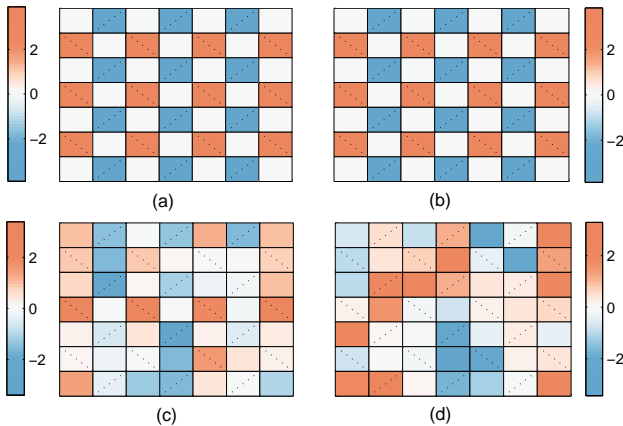


FIG. 7. (Color online) Snapshot depicting the circulation of flux, clockwise or anticlockwise, on each plaquette of 8×8 lattice for different values of magnetic field (a) $h^z = 0.0$, (b) $h^z = 0.8$, just before the phase transition (c) $h^z = 1.2$, just after phase transition (d) $h^z = 1.6$, when almost all spins become parallel with h -field. The different parameters used in the calculations are same as mentioned in Fig. 6.

V. SUMMARY

To summarize, we have studied the Kondo lattice model with additional DM interaction on the Shastry-

Sutherland lattice. Our results show that complex, non-coplanar spin configurations can be generated dynamically from purely short range interactions and coupling to itinerant electrons. We conclude that DM interactions are necessary for the emergence of chiral spin configurations when the electronic spectrum is gapped, that is, the system is in an insulating state. We have carefully identified the minimal DM vectors necessary for the stabilization of non-coplanar configurations as well as for the appearance of magnetization plateaus in the presence of such topologically non-trivial configurations of the local moments. Furthermore, such non-coplanar structures can be tuned continually by applying an external magnetic field. These results provide an insight into the origin and nature of topologically non-trivial magnetic phases in metallic magnets. They will also be crucial in understanding the magnetic and electronic properties of the rare earth tetraboride family of metallic frustrated magnets.

ACKNOWLEDGMENTS

It is a pleasure to thank G. Alvarez and Y. Kato for useful discussions on the development of the numerical method. The work is partially supported by Grant No. MOE2014-T2-2-112 from the Ministry of Education, Singapore.

- ¹ I. Martin and C. D. Batista, *Phys. Rev. Lett.* **101**, 156402 (2008).
- ² K. Barros, J. W. F. Venderbos, G.-W. Chern, and C. D. Batista, *Phys. Rev. B* **90**, 245119 (2014).
- ³ H. Ishizuka and Y. Motome, *Phys. Rev. B* **88**, 081105 (2013).
- ⁴ G.-W. Chern, *SPIN* **05**, 1540006 (2015).
- ⁵ Y. Kato, I. Martin, and C. D. Batista, *Phys. Rev. Lett.* **105**, 266405 (2010).
- ⁶ Y. Machida, S. Nakatsuji, Y. Maeno, T. Tayama, T. Sakakibara, and S. Onoda, *Phys. Rev. Lett.* **98**, 057203 (2007).
- ⁷ S. Nakatsuji, Y. Machida, Y. Maeno, T. Tayama, T. Sakakibara, J. v. Duijn, L. Balicas, J. N. Millican, R. T. Macaluso, and J. Y. Chan, *Phys. Rev. Lett.* **96**, 087204 (2006).
- ⁸ M. Udagawa and R. Moessner, *Phys. Rev. Lett.* **111**, 036602 (2013).
- ⁹ G.-W. Chern, *Phys. Rev. Lett.* **105**, 226403 (2010).
- ¹⁰ Y. Akagi and Y. Motome, *J. Phys.: Conf. Ser.* **320**, 012059 (2011).
- ¹¹ Y. Akagi, M. Udagawa, and Y. Motome, *Phys. Rev. Lett.* **108**, 096401 (2012).
- ¹² J. W. F. Venderbos, M. Daghofer, J. van den Brink, and S. Kumar, *Phys. Rev. Lett.* **109**, 166405 (2012).
- ¹³ R. Karplus and J. M. Luttinger, *Phys. Rev.* **95**, 1154 (1954).
- ¹⁴ J. Ye, Y. B. Kim, A. J. Millis, B. I. Shraiman, P. Majumdar, and Z. Tešanović, *Phys. Rev. Lett.* **83**, 3737 (1999).
- ¹⁵ D. Xiao, M.-C. Chang, and Q. Niu, *Rev. Mod. Phys.* **82**, 1959 (2010).
- ¹⁶ Y. Taguchi, Y. Oohara, H. Yoshizawa, N. Nagaosa, and Y. Tokura, *Science* **291**, 2573 (2001).
- ¹⁷ B. S. Shastry and B. Sutherland, *Physica B+C* **108**, 1069 (1981).
- ¹⁸ P. Coleman and A. H. Nevidomskyy, *J. Low Temp. Phys.* **161**, 182 (2010).
- ¹⁹ B. H. Bernhard, B. Coqblin, and C. Lacroix, *Phys. Rev. B* **83**, 214427 (2011).
- ²⁰ J. H. Pixley, R. Yu, and Q. Si, *Phys. Rev. Lett.* **113**, 176402 (2014).
- ²¹ L. Su and P. Sengupta, *Phys. Rev. B* **92**, 165431 (2015).
- ²² K. Siemensmeyer, E. Wulf, H.-J. Mikeska, K. Flachbart, S. Gabáni, S. Mat'aš, P. Priputen, A. Efdokimova, and N. Shitsevalova, *Phys. Rev. Lett.* **101**, 177201 (2008).
- ²³ K. Wierschem, S. S. Sunku, T. Kong, T. Ito, P. C. Canfield, C. Panagopoulos, and P. Sengupta, *Phys. Rev. B* **92**, 214433 (2015).
- ²⁴ S. S. Sunku, T. Kong, T. Ito, P. C. Canfield, B. S. Shastry, P. Sengupta, and C. Panagopoulos, *Phys. Rev. B* **93**,

²⁵ 174408 (2016).

²⁵ T. Suzuki, Y. Tomita, N. Kawashima, and P. Sengupta, *Phys. Rev. B* **82**, 214404 (2010).

²⁶ S. Mat'a, K. Siemensmeyer, E. Wheeler, E. Wulf, R. Beyer, T. Hermannsdrfer, O. Ignatchik, M. Uhlzarz, K. Flachbart, S. Gabni, P. Priputen, A. Efdokimova, and N. Shitsevalova, *J. Phys. Conf. Ser.* **200**, 032041 (2010).

²⁷ T. Suzuki, Y. Tomita, and N. Kawashima, *Phys. Rev. B* **80**, 180405 (2009).

²⁸ F. Iga, A. Shigekawa, Y. Hasegawa, S. Michimura, T. Takabatake, S. Yoshii, T. Yamamoto, M. Hagiwara, and K. Kindo, *J. Magn. Magn. Mater.* **310**, e443 (2007), proceedings of the 17th International Conference on MagnetismThe International Conference on Magnetism.

²⁹ S. Michimura, A. Shigekawa, F. Iga, T. Takabatake, and K. Ohoyama, *J. Phys. Soc. Jpn.* **78**, 024707 (2009).

³⁰ H. Ishizuka and Y. Motome, *Phys. Rev. Lett.* **108**, 257205 (2012).

³¹ H. Ishizuka and Y. Motome, *Phys. Rev. B* **87**, 081105 (2013).

³² H. Ishizuka and Y. Motome, *Phys. Rev. B* **91**, 085110 (2015).

³³ Y. Motome and N. Furukawa, *J. Phys. Soc. Jpn.* **68**, 3853 (1999).

³⁴ N. Furukawa and Y. Motome, *J. Phys. Soc. Jpn.* **73**, 1482 (2004).

³⁵ Kumar, S. and Majumdar, P., *Eur. Phys. J. B* **50**, 571 (2006).

³⁶ A. Mukherjee, N. D. Patel, C. Bishop, and E. Dagotto, *Phys. Rev. E* **91**, 063303 (2015).

³⁷ S. Kumar and P. Majumdar, *Phys. Rev. Lett.* **96**, 016602 (2006).

³⁸ S. Kumar and P. Majumdar, *Phys. Rev. Lett.* **94**, 136601 (2005).